Iranian Journal of Materials Forming 14 (1) (2027) 55-72

Online ISSN: 2383-0042

IJMF

Iranian Journal of Materials Forming

Journal Homepage: http://ijmf.shirazu.ac.ir

Research Article

Investigating the Effect of Strain on Deformation Behavior and Microstructural Evolutions During Non-Isothermal Hot Compression of Ti-6Al-4V Alloy

Mahnaz Jafari[1], Gholamreza Ebrahimi[1*], Seyed Mahmood Fatemi[2], Amir Momeni[3] and Mohammad Mazinani[1]

[1] Department of Materials Science and Engineering, Faculty of Engineering, Ferdowsi University of Mashhad, Mashhad, Iran
[2] Department of Materials Science and Engineering, Universitat Politècnica de Catalunya-BarcelonaTech, Campus Diagonal Besòs-EEBE, 08019 Barcelona, Spain
[3] Department of Materials Science and Engineering, Hamedan University of Technology, Hamedan, Iran

ARTICLE INFO

Article history:

Received: 15 April 2026
Reviewed: 1 June 2026
Revised: 12 June 2026
Accepted: 23 June 2026

Keywords:

Hot deformation
Non-isothermal compression
Spheroidization
Ti-6Al-4V alloy
Secondary alpha

Please cite this article as:

Jafari, M., Ebrahimi, G., Fatemi, S. M., Momeni, A., & Mazinani, M. (2027). Investigating the effect of strain on deformation behavior and microstructural evolutions during non-isothermal hot compression of Ti-6Al-4V alloy. *Iranian Journal of Materials Forming*, *14*(1), 55-72. https://doi.org/10.22099/ijmf.2026.55932.1379

ABSTRACT

Ti-6Al-4V alloy is a two-phase alloy that has excellent mechanical properties and good corrosion resistance. This alloy is widely used in the manufacture of aircraft engine components such as fan blade frames and fan discs. In the present study, the non-isothermal deformation behavior of Ti-6Al-4V alloy and the effect of strain on its microstructural evolution were investigated. For this purpose, samples were compressed at a constant strain rate of 0.01 s^{-1} under non-isothermal conditions with a cooling rate of about 0.6 °C/s, starting from 950 °C. The effect of increasing strain on the volume fraction of secondary alpha lamellae, their aspect ratio, and their thickness was examined by interrupting the test at strain levels of 0.2, 0.4, and 0.8. The results showed that during non-isothermal deformation, the volume fraction of the secondary alpha lamellae increases significantly with increasing applied strain. Regardless of the temperature drop, deformation promotes the formation of numerous fine needle-shaped secondary alpha lamellae. The microstructural observations showed that the volume fraction of alpha lamellae increased by about 10.5%, in the sample deformed to a strain of 0.8. As the strain increases, the aspect ratio of the secondary alpha lamellae decreases. At a strain of 0.8, 54% of the alpha lamellae exhibit an aspect ratio of less than 2.5. At low applied strains (up to 0.4), the dominant effect of strain is the increase in the volume fraction of secondary alpha, and the prevailing mechanism of alpha-lamella spheroidization is the fragmentation of the lamellae through buckling. However, at higher strains (0.4-0.8), the dominant deformation mechanism shifts, and spheroidization of the alpha lamellae mainly occurs through the formation of thermal grooves and boundary splitting. In addition, at low strains (0.2-0.4), both the formation rate of secondary alpha lamellae and their spheroidization rate are higher than those observed at larger strains (0.4-0.8).

© Shiraz University, Shiraz, Iran, 2027

1. Introduction

The combination of high specific strength, low density, excellent corrosion resistance, and good toughness has made Ti alloys highly attractive materials for the aerospace industry [1, 2, 6, 7]. They account for approximately 30-50 percent of the total weight of

* Corresponding author
E-mail address: r.ebrahimi@um.ac.ir (G. Ebrahimi)
https://doi.org/10.22099/ijmf.2026.55932.1379

Published by Shiraz University. This is an open access article under the CC BY-NC-ND license (http://creativecommons.org/licenses/by-nc-nd/4.0/).

advanced aircraft, including turbine components. Hot forging is the most common forming route for titanium alloy components in industry [1, 2]. Dual-phase Ti alloys, which consist of α with HCP and β with BCC crystal structures, have shown excellent performance in aerospace applications. Fine equiaxed α grains in a transformed β matrix can offer an excellent combination of ductility, toughness, fatigue and creep resistance in dual-phase Ti alloys [8, 18]. Ti-6Al-4V alloy is a two-phase alloy that exhibits excellent mechanical properties and good corrosion resistance. This alloy is widely used in the manufacture of aircraft engine components such as fan blade frames and fan discs [30]. To achieve the desired duplex structure, isothermal hot deformation is often conducted in the two-phase region to break the α layers and transform them into equiaxed grains. However, under industrial production conditions, strictly isothermal deformation is often difficult to maintain and the products are therefore frequently fabricated under non-isothermal conditions. The temperature drop during deformation leads to complex phase transformations, which significantly affect the morphology and phase fraction of the final microstructure [19]. The final microstructure obtained under non-isothermal deformation condition depends strongly on the processing parameters, including deformation temperature, strain and strain rate. To date, limited studies have been devoted to the microstructural evolutions of Ti alloys under non-isothermal deformation conditions. Fan et al. [12] investigated the effect of strain and cooling rate on the evolution of primary and secondary alpha phases during non-isothermal deformation. Their results showed that the growth of the primary α is delayed, while the precipitation of secondary α is enhanced during deformation under low cooling rates. Li et al. [13] investigated the effect of non-isothermal deformation on the microstructure of Ti-6Al-2.5V-1.5Cr-0.5Fe-0.3Si alloy under different cooling rates. The results showed that the secondary α phase significantly precipitates during cooling below a certain temperature. In another study, Li et al. [20] investigated the evolution of secondary α in TC6 alloy with different strains and cooling conditions under non-isothermal deformation. Their results indicated that under non-isothermal deformation, the volume fraction of αs increases significantly. Furthermore, when the material is cooled without deformation, the Burgers orientation relationship between secondary α and β is maintained. However, by applying non-isothermal deformation, the Burgers orientation relationship between secondary α with β is lost, helping the secondary α precipitates to become equiaxed. Chen et al. [9] investigated the microstructure and texture evolution of Ti-7333 alloy and showed that hot deformation under non-isothermal condition has a negative effect on the precipitation of secondary α. Meng et al. [39] showed that there is a competition between the precipitation of secondary α and the growth of primary one in two-phase Ti alloys. Their results for TA15 titanium alloy with an initial equiaxed microstructure, showed that the secondary α nucleates at the interface between the equiaxed primary α and the β matrix, during continuous cooling.

Due to the wide applications of Ti-6Al-4V alloy in aerospace applications [44, 46], its microstructural evolution through thermomechanical processes [5, 39, 44] have been sufficiently studied. In these studies, the effects of deformation variables, under isothermal conditions, on the evolutions of microstructural components including transformed β and α, have been investigated. Despite the available literature on this topic, the effect of deformation parameters, i.e. strain, strain rate, and cooling rate on the microstructural evolution, particularly the formation of equiaxed α during non-isothermal hot deformation of α+β duplex structures in Ti alloys, has not been sufficiently characterized. Hence, the aim of the present study was to investigate the effect of strain during non-isothermal hot compression on the deformation behavior and the related microstructural evolution in Ti-6Al-4V alloy. It is expected that the results of this study will provide a better understanding of the relationship between flow behavior and microstructure evolution and assist industry in the design of non-isothermal hot working processes for Ti-6Al-4V alloy.

2. Materials and Methods

The chemical composition of Ti-6Al-4V alloy, used in this investigation is presented in Table 1. The material was supplied as extruded rod and then cut into cylindrical samples with the dimensions of 10×15 mm using electrical discharge machining (EDM) equipment.

The β transformation temperature of the Ti-6Al-4V alloy was to be approximately 980 °C using differential thermal analysis (DTA), corresponding DTA curve is presented in in Fig. 1.

A preliminary heat treatment, known as β annealing, was performed on the samples at 1030 °C for 5 minutes to ensure complete β transformation and microstructural homogenization. Following homogenization, the samples were rapidly quenched in water to obtain a fine fully lamellar microstructure containing α layers. For the non-isothermal hot compression tests, the quenched samples were heated again to 950 °C (within the α+β two-phase region) at a heating rate of 10 °C/s and held for 5 minutes to obtain a duplex microstructure.

The samples were then subjected to non-isothermally hot compressed at a strain rate of 0.01 s^{-1} to true strains of 0.2, 0.4, and 0.8, corresponding to the instant temperatures of 936, 925, and 905 °C, respectively. After reaching the required strain values, the deformed samples were rapidly quenched to ambient temperature. To characterize the microstructure immediately before the compression tests, a witness sample was directly quenched after holding at 950 °C for 5 minutes. Fig. 2 shows the schematic diagram of the thermomechanical schedule applied to the samples. A Zwick/Roell thermomechanical simulator was used to perform the hot compression tests under continuous cooling according to the cooling schedule shown in Fig. 3. Based on Fig. 3, the average cooling rate was approximately 0.6 °C/s.

In order to separate the effects of deformation and cooling on microstructural evolution during non-isothermal deformation, witness specimens were subjected only to the same cooling regime, as shown in Fig. 2, without applying deformation.

The deformed and witness samples were then cut along their vertical axis and prepared by the standard metallographic techniques. After mechanical polishing with a suspension composed of 3 g Al_2O_3, 2 ml HNO_3, 100 ml H_2O, and 0.3 ml HF, the samples were etched using Kroll's etchant. Microstructural characterizations were performed using an optical microscope (Olympus GX51) and a scanning electron microscope (TESCAN-

Table 1. Chemical composition of Ti-6Al-4V alloy (wt.%)

Al	V	Fe	C	N	O	H	Ti
6.2	4.1	0.2	0.01	0.01	0.15	0.001	Balance

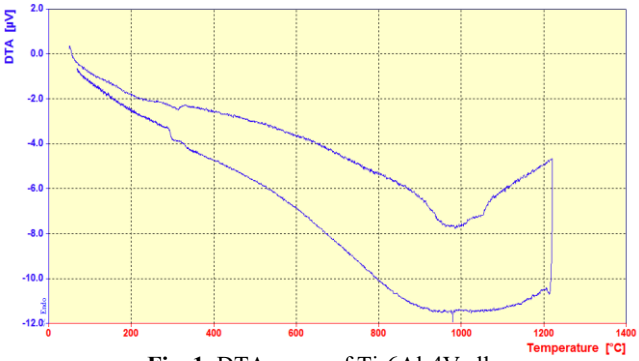

Fig. 1. DTA curve of Ti-6Al-4V alloy.

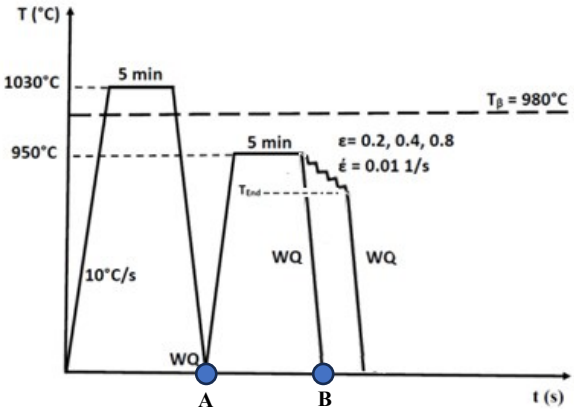

Fig. 2. Schematic of the thermomechanical regime applied to the samples in this research.

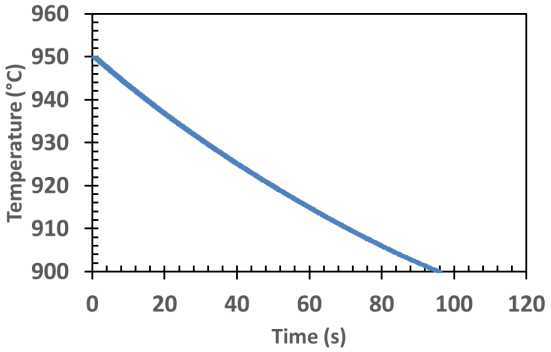

Fig. 3. Cooling curve applied to the samples through the non-isothermal compression tests.

XMU). For quantitative microstructural analyses, including the evaluation of phase fractions, aspect ratio, and grain size, ImageJ software was used. For each condition, the measurements were repeated three times and the average results was reported. For the witness samples the changes in the volume fraction of the α and β phases during cooling were determined using JMat Pro software.

3. Results and Discussion

3.1. Microstructural characterization

The microstructure of the material after β annealing is shown in Fig. 4. It is evident that annealing at high temperature causes considerable grain coarsening, such that the average prior β grain size increased to approximately 950 µm. This microstructure, which consists of α layers and transformed β within the large prior β grains [27], provides the conditions for the globularization of the α phase and the formation of an equiaxed microstructure during non-isothermal deformation in the two-phase region. The optical micrograph of the witness sample after holding for 5 minutes at 950 °C and quenching, together with the continuous cooling-transformation (CCT) curves of the alloy is shown in Fig. 5.

As shown in Fig. 5(a), after holding the β-annealed microstructure (Fig. 4) at 950 °C for 5 minutes, a two-phase α+β microstructure containing three different morphologies of primary α (α_p) is formed within the β matrix. As observed, the primary α phase exhibits different morphologies, including equiaxed, lamellar

Fig. 4. Microstructure of Ti-6Al-4V alloy after β annealing treatment (point A in Fig. 2).

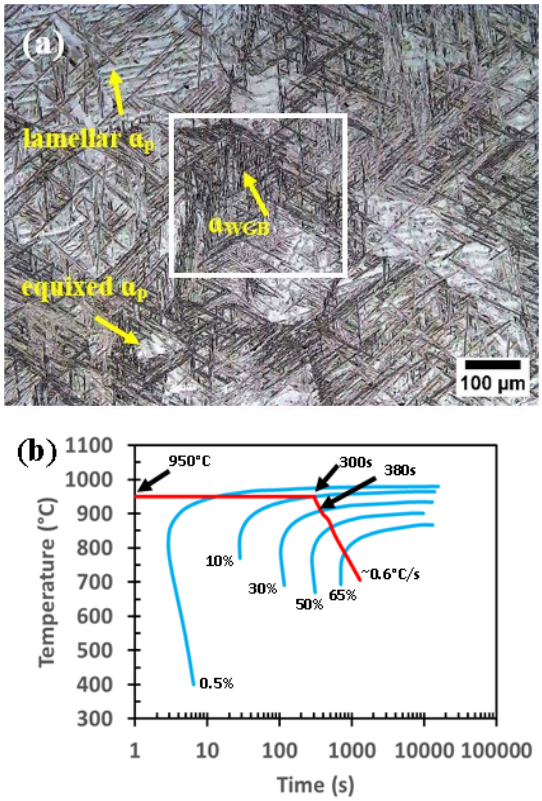

Fig. 5. (a) Optical micrograph of the witness sample after holding 950 °C for 5 minutes and quenching (point B in Fig. 2) and (b) continuous cooling transformation (CCT) diagram of Ti-6Al-4V alloy calculated using JMatPro software.

and newly formed needle-like α. As highlighted by the rectangle in Fig. 5(a), the acicular α phases is clearly distinguished from the dark retained β phase. It is evident that the acicular α needles nucleate predominantly at the prior β grain boundaries and grow into the β matrix with a morphology similar to that of the Widmanstätten phase [11]. Therefore, they are designated as α_{WGB} in Fig. 5(a). The nucleation and growth of α_{WGB} are accompanied by the diffusion of α stabilizer elements, such as Al, O, N, and C, toward the needles, while β-stabilizer elements, such as Mo, Nb, V, and Fe, diffuse away from them [12-16]. High temperature annealing, e.g. annealing at 950 °C, facilitates the rapid diffusion of these elements, creating suitable conditions for the nucleation of grain boundary Widmanstätten α phase. Fig. 5(b) shows the CCT diagram for the Ti-6Al-4V alloy, calculated using JMatPro software. The straight line drawn in Fig. 5(b) represents the heat treatment of the sample at 950 °C for

5 minutes (300 seconds). Hence, the CCT curve predicts the formation of approximately 10% α phase during the isothermal treatment at 950 °C for 5 minutes. This corresponds to the primary α phase formed in the equiaxed and lamellar morphologies around the prior β grain boundaries in Fig. 5(a). The formation of α_p nuclei help decrease the total excessive energy of the grain boundary regions. According to Fig. 5(b), although a longer holding time increases the fraction of α_p, it also leads to excessive coarsening of the primary nuclei, which is undesirable. Hence, it is preferable that a larger fraction of α phase, referred to as secondary α (α_s), forms during post-annealing cooling. The preferred nucleation sites for the secondary α phase are the interfaces between the primary α phase and the β matrix. The lamellar shape is the preferential morphology of α_s [17]. As shown in Fig. 5(b), continuous cooling at an average rate of 0.6 °C/s increases the total α α-phase fraction through the progressive formation of α_s. To quantify the phase fractions of α and β during continuous cooling of the witness sample, simulations were performed using JMatPro software. The variations in the α and β phase fractions of the witness sample cooled according to the schedule shown in Figs. 3 and 5(b) are presented in Fig. 6.

Fig. 6 indicates that the total α-phase (primary + secondary) increases monotonically to approximately 90%, whereas the β-phase fraction decreases to approximately 10% at low temperatures. In the current research, continuous cooling was applied to the finishing temperatures of 936, 925, and 905 °C, corresponding to true strain values of 0.2, 0.4, and 0.8, respectively, after which the samples were quenched in water to ambient temperature (Fig. 2). Hence, the phase fractions of α and β in the witness sample at the initial cooling temperature, (950 °C) and at the finishing temperatures of 936, 925, and 905 °C were extracted from Fig. 6 and are summarized in Table 2.

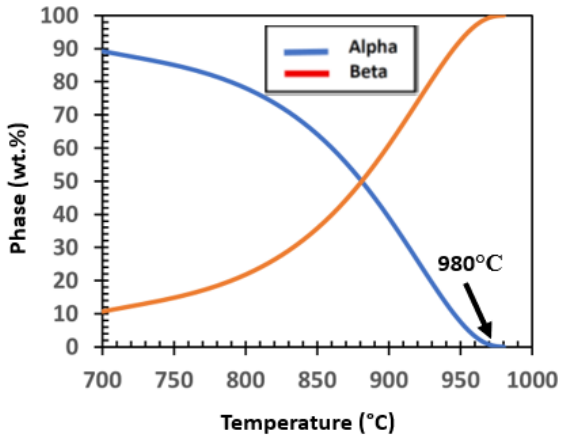

Fig. 6. Changes in the phase fractions of α and β with temperature during cooling at a rate of 0.6 °C/s, calculated using JMat Pro software.

The results of Fig. 6 and Table 2 help to identify the effect of the thermal cycle applied to the samples (Figs. 2 and 5(b)) on the phase fractions of the α and β phases, regardless of deformation. Based on the values reported in Table 2, the amount of α phase increases by about 113%, 201%, and 377% through continuous cooling to 936, 925, and 905 °C, respectively. As discussed, α_s with the preferential lamellar morphology forms during continuous cooling in the two-phase region. Therefore, the comparison of the α fraction at 950 °C and lower temperatures in Table 2 indicates that the lamellar morphology should constitute the major portion of the total α fraction in the microstructure.

Fig. 7 displays the microstructure of the samples non-isothermally deformed to true strains of 0.2, 0.4, and 0.8 at strain rate of 0.01 s^{-1}. As discussed before, the non-isothermal deformation started at 950 °C, and the temperature decreased according to the cooling regime shown in Fig. 3. To reach the true strain values of 0.2, 0.4, and 0.8, the temperature decreased to 936, 925, and 905 °C, respectively. Fig. 7(a) indicates that after a true strain of 0.2, a small number of α_s lamellae have formed. The shortness of some of these lamellae can be attributed to the limitation of their growth caused by impingement with other lamellae. The α_p layers seem to act as the preferential nucleation sites for them. In Fig. 7(a), the α_s

Table 2. Phase fractions of the witness sample at the initial and finishing temperatures of the cooling curve (Fig. 3). The data were extracted from Fig. 5

Temperature (°C)	Phases (wt.%)	
	α	β
950	7.5	92.5
936	16	84
925	22.6	77.4
905	35.8	64.2

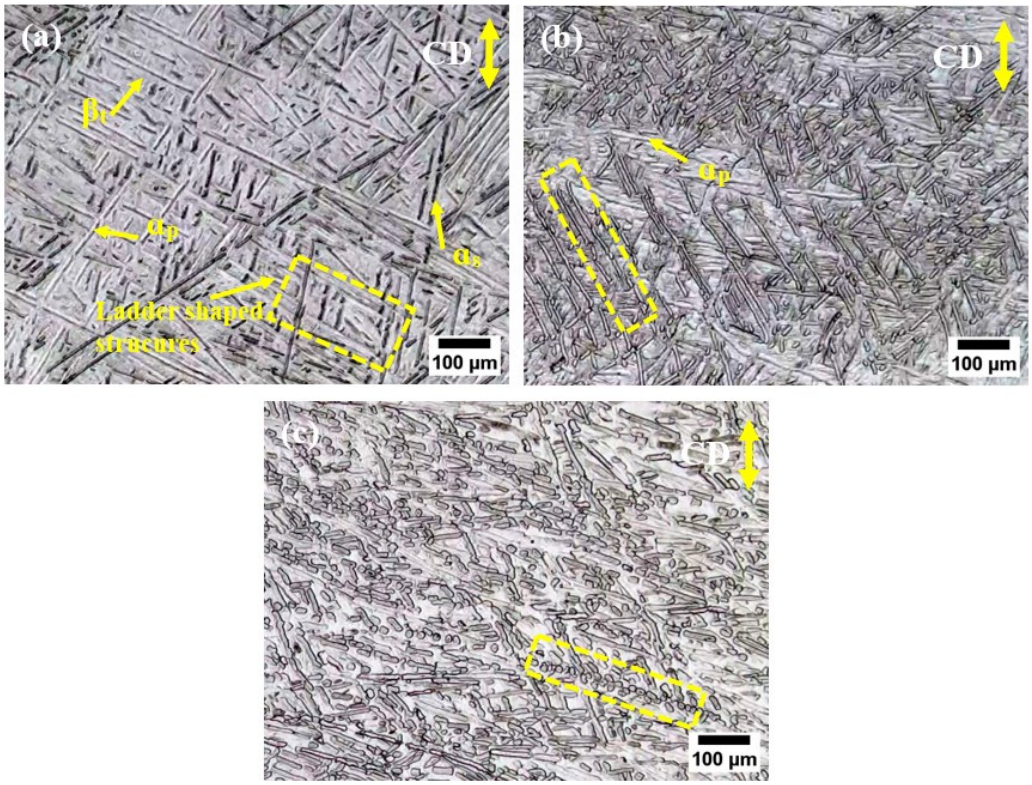

Fig. 7. Microstructure of Ti-6Al-4V after non-isothermal deformation at a strain rate of 0.01 s^{-1} to strain values of (a) 0.2, (b) 0.4, and (c) 0.8. "CD" on the top right-hand of the micrographs denotes the hot compression direction.

lamellae can be distinguished from the α_p ones by their darker appearance. This is attributed to the difference in the chemical compositions of α_s and α_p [10, 28].

When some short α_s short lamellae nucleate between longer α_p lamellae, a ladder-like structure is formed, as shown by the yellow dashed rectangle in Fig. 7(a). In such structures, α_p lamellae form the ladder rails, and the α_s lamellae constitute the rungs. The matrix in Fig. 7(a) is transformed β, including the bright Widmanstätten needles of α_p with thicker appearance and thinner α_s lamellae. At $\varepsilon = 0.2$, the α_p lamellae (bright lamellae) show slight rotation and tilting perpendicular to the compression axis. However, there is no significant morphological change or breaking in the α_s lamellae. This suggests that the strain was insufficient to initiate significant breaking and fragmentation of the α layers required to form a duplex structure. As observed in Fig. 5(b), the cooling curve at a true strain of 0.2, i.e. 20 seconds after the onset of deformation at 950 °C, or 320 seconds from the start of the two-phase annealing process, lies between the transformation curves of 10% and 30% α, where the temperature decreases to about 936 °C. Fig. 5(b) indicates that the total phase percentage of α increases to about 16% with the decrease in temperature to 936 °C, regardless of the effect of applied deformation. Since, referring to Table 2, 7.5% of the total fraction of α (16%) is α_p, the portion of α_s, formed through continuous cooling is estimated to be about 8.5%. Based on Table 2, with a further increase in strain to 0.4 and a decrease in temperature to 925 °C, the fraction of α_s significantly increases to 15.1% (= 22.6-7.5%). This is readily observed from the comparison between Figs. 7(a) and 7(b). At $\varepsilon = 0.4$, breaking and fragmentation are observed in many α_s lamellae. An example of the fragmentation of α_s lamellae is highlighted within the yellow rectangle in Fig. 7(b). In addition to the lamellae fragmentation in α_s, the reorientation perpendicular to the compression axis is the major microstructural change observed in the α_p lamellae. Due to the microstructural evolutions in α_s and α_p, $\varepsilon = 0.4$ can be considered the critical strain for the onset of spheroidization of α and the formation of an

equiaxed duplex structure. The strain of 0.4 was also reported as the critical strain for the start of dynamic globularization in Ti-6Al-4V alloy by Kedial et al. [18]. At lower strains, such as ε = 0.2, the volume fraction of α is much lower than that of β and this postpones the morphological changes in α. In two-phase materials, the total strain is distributed between the constituent phases in proportion to their volume fractions. This phenomenon is described by the mixture rule, given by:

$$\varepsilon = f_\alpha \varepsilon_\alpha + f_\beta \varepsilon_\beta \quad (1)$$

Where f_a and f_β are the volume fractions of the alpha and beta phases, respectively, ε_a and ε_β are the strains tolerated by the alpha and beta phases. Eq. (1) shows that a phase with a higher volume fraction is subjected to a higher strain. Moreover, the strain partitioning between phases is significantly dependent on their intrinsic mechanical behavior. The α phase due to its HCP crystal structure is much harder than the β phase, which has a BCC structure under hot working conditions. Therefore, α tends to bear lower strain when it coexists with β in two-phase Ti alloys. Referring to Eq. (1), since $\varepsilon_\alpha < \varepsilon_\beta$, to increase the total strain accommodated by the α phase, it is necessary to increase f_α.

At strains lower than 0.4, the volume fraction of α lamellae (the harder phase) is very low (8.5% at ε = 0.2) and thus the strain accommodated by the α layers is very small compared to that of β [19]. Low strain values in α only activate the primary microstructural mechanisms such as the formation of low angle grain boundaries (LAGBs) and rotation of alpha layers towards the direction perpendicular to the compression direction [19-21]. The reorientation of α lamellae is observed partly in Fig. 7(b) and becomes more pronounced in Fig. 7(c). As the strain increases, moving dislocations in the α_s lamellae progressively join the LAGBs and gradually transform them into high angle grain boundaries (HAGBs), which can provide pathways for the diffusion of β into α layers to fragment them [22]. In this process, the crystallographic orientation of α lamellae plays a crucial role; such that layers with more favorable orientations and a higher Schmid factor undergo greater stress concentration. These layers exhibit more dislocation activity and a higher degree of spheroidization [23, 24]. Under non-isothermal deformation conditions, medium strain values provide the most suitable condition for microstructural evolution [5, 25]. This is because, at high strain values, the corresponding decrease in temperature significantly increases the fraction of α_s lamellae and thus decreases the space between them. In this situation, the small distance between the layers makes the strain transfer from the matrix to the layer very difficult and postpones the fragmentation and spheroidization mechanisms.

Since, ε = 0.8 corresponds to 80 seconds after the onset of deformation at 950 °C or 380 seconds from the start of the two-phase annealing process, according to the cooling regime shown in Fig. 3, the temperature of the sample falls to about 905 °C. Thus, based on Table 2 and Fig. 5(b), the fraction of α_s is estimated to be 28.3% (= 35.8-7.5), which presents an increase of about 87% and 233% over the α_s fraction obtained after strains of 0.4 and 0.2, respectively. Fig. 7(c) shows that most of the α lamellae have broken and fragmented into shorter segments, and the long layers in Figs. 7(a) and (b) are no longer evident. As shown by the yellow rectangle, some α layers have become completely spheroidized. Many α lamellae with an orientation angle of about 70° between them and the compression axis in Fig. 7(c) have been completely fragmented (for example, the alpha layer located in the yellow rectangle). It confirms that the orientation angle of α lamellae is an important factor in facilitating their spheroidization under non-isothermal hot compression.

Fig. 8 displays the SEM images of the microstructures of samples deformed to strains of 0.2, 0.4, and 0.8. In agreement with Fig. 7(a), Fig. 8(a) indicates that the microstructure of the sample deformed to a strain of 0.2 includes α_p layers with a gray color, α_s layers with a dark color and thin bright layers of retained β around both the α_p and α_s layers. In addition to the longer α_s layers, the formation of some finer layers, shown by the yellow arrow indicates that the α_s layers are effectively refined by deformation. Fig. 8(a) indicates that deformation up to a strain of 0.2 does not

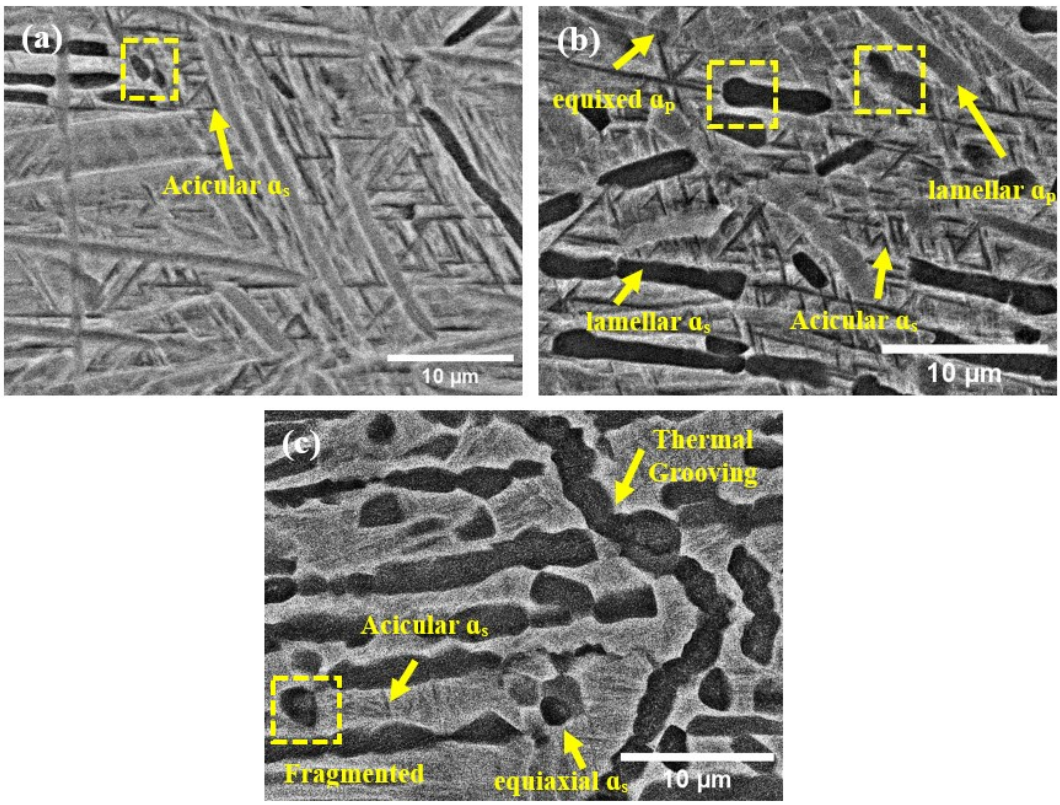

Fig. 8. SEM micrographs of the microstructure of samples, non-isothermally deformed at a strain rate of 0.01 s^{-1} to true strains of (a) 0.2, (b) 0.4, and (c) 0.8.

produce a significant change in the morphology of α_p, and the lamellar structure remains nearly unchanged with smooth boundaries.

With the increase in strain to 0.4 (Fig. 8(b)), the fraction of α_s layers (dark layers) and the total fraction of α phase ($\alpha_p + \alpha_s$) significantly increases. It is also obvious that deformation decreases the aspect ratio (width to length ratio) of α_s layers. On the other hand, Fig. 8(b) indicates that after deformation up to a strain of 0.4, the morphology and fraction of α_p lamellae remain nearly unchanged. Therefore, it is inferred that deformation under non-isothermal conditions shifts the competition between α_s precipitation and α_p growth in favor of α_s precipitation.

Fig. 8(b) clearly shows the appearance of thermal grooving and edge nucleation (shown by the dashed rectangles), which are the sub-mechanisms of fragmentation and spheroidization of α_s lamellae [26]. Thermal grooving and edge nucleation contribute to the splitting and fragmentation of the α_s lamellae. The fragmented layers eventually undergo spheroidization through termination migration or Ostwald ripening mechanisms. In the termination migration mechanism, diffusion of elements occurs from the layer ends to the central parts due to the chemical potential difference caused by curvature variations. In contrast, during the Ostwald ripening mechanism, larger fragments of the layers become spherical at the expense of consuming smaller fragments [3, 26]. In agreement with the previous results in Fig. 7, the limited occurrence of thermal grooving in Fig. 8(b) (shown by the yellow rectangles), confirms that $\varepsilon = 0.4$ is the critical strain for the initiation of dynamic fragmentation and spheroidization of α in Ti-6Al-4V alloy. Therefore, it can be stated that at $\varepsilon < 0.4$, strain mainly contributes to the increase in the fraction of needle-shaped α_s and at $\varepsilon \geq 0.4$, strain activates the fragmentation and spheroidization of the same needle-shaped α_s to form an equiaxed duplex structure at larger strains. With the increase in strain to 0.8 (Fig. 8(c)), almost all of the α_s layers exhibit thermal grooving and β has locally penetrated into the α_s layers. In some cases, shown by

the yellow rectangle, thermal grooves with greater penetration of β have fragmented the α_s layer. Some of the equiaxed alpha grains formed through this mechanism are indicated by arrows in Fig 8(c). Although the needle-shaped α_s layers are still distinguishable in Fig. 8(c), their phase fraction does not show a significant change, comparing with Fig. 8(b). This indicates that in the strain range of 0.4-0.8, most of the deformation energy, applied to the sample was spent on activating the thermal grooves and fragmenting the α_s layers and the rate of secondary alpha formation decreases. Lower temperatures at high strains both slow down the diffusion of elements and, because a large amount of the matrix supersaturation has been consumed by the time those strains are reached, reduce the rate of secondary alpha formation, for example, at a strain of 0.8. In addition to these two main factors, the increase in the percentage of alpha at a strain of 0.8, due to the principle of strain division, leads to a decrease in the stress on the beta phase and, as a result, a slowdown in the rate of secondary alpha formation. In other words, during non-isothermal hot deformation, strains up to 0.4 are required to increase the volume fraction of α_s needles and layers; strains in the range of 0.4-0.8 activate the micro-mechanisms of fragmenting the α_s layers and therefore additional strain is required to cause the spheroidization of fragmented α_s layers and to form a fully equiaxed duplex structure. In the last step of this process, i.e. spheroidization, diffusion of elements occurs from the α layer to the fragmented regions by the thermal grooves [4, 37]. This diffusion scenario is supported by the boundary curvature, which is called the "Ostwald ripening mechanism". Finally, the larger fragments become spherical at the expense of smaller ones [3].

Fig. 9 shows the SEM micrograph of the microstructure of the witness sample, subjected to the cooling regime, shown in Fig. 2, without deformation. The witness sample was annealed at 950 °C for 5 minutes and then cooled to 905 °C, within 80 seconds (equivalent to a strain of 0.8). A comparison of Figs. 9 and 8(c), indicates some differences between the microstructure of the witness sample and the microstructure of the sample deformed to ε = 0.8. First, although acicular α_s layers are abundant in Fig. 8(c), only a few of them are observed in Fig. 9.

This indicates that deformation has a significant effect on the formation of secondary α_s. Deformation introduces more nucleation sites for the precipitation of secondary phases in the matrix. The population of dislocations, shear bands, deformation bands and sub-boundaries can facilitate the formation of α_s in a deformed $\alpha_p + \beta_t$ matrix [7, 8]. Second, in contrast to the fragmentation and spheroidization mechanism observed in Fig. 8(c), the α_s layers are nearly unchanged after cooling in the witness sample (Fig. 9). It is inferred that the microstructural evolution of α_s, which causes a morphological change from the lamellar structure of α + β to the equiaxed one, are mainly activated by strain and cooling is not the main factor. To further elucidate the effect of strain on the morphological evolution of α_s, the variations in the aspect ratio (AR), volume fraction, and thickness of the α_s layers are investigated in the next section.

3.2. Effect of non-isothermal deformation on the α_s layers

The effect of non-isothermal deformation on the morphology and AR (= length/width ratio) of α_s layers in the deformed samples is shown in Fig. 10. The SEM micrographs of samples deformed to strains of 0.2, 0.4, and 0.8 are shown in Figs. 10(a-c) and the corresponding

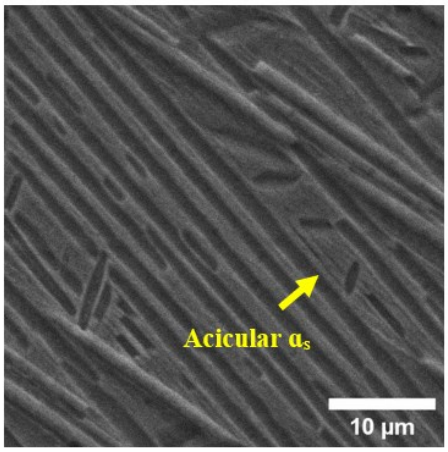

Fig. 9. SEM micrograph of the microstructure of the witness sample after cooling for 80 seconds from the starting temperature of 950 °C to the final temperature of 905 °C and then quenching to ambient temperature.

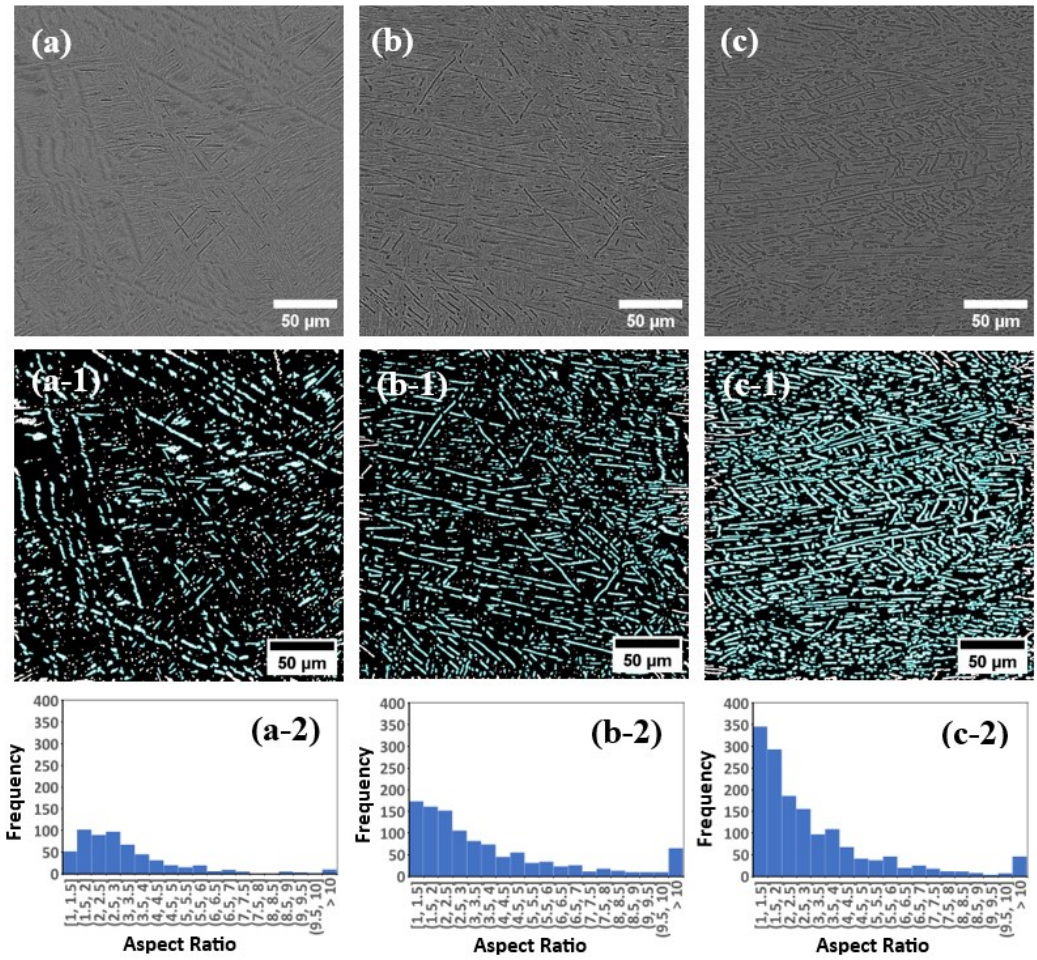

Fig. 10. SEM micrographs of the microstructures of samples, non-isothermally deformed at a strain rate of 0.01 s^{-1} to strains of (a) 0.2, (b) 0.4, and (c) 0.8. The binary images used to calculate the aspect ratio of the alpha layers by ImageJ software for (a), (b), and (c) are presented in (a-1), (b-1), and (c-1), respectively. The aspect ratio frequency histograms of the alpha layers for (a-1), (b-1), and (c-1) are shown in (a-2), (b-2), and (c-2), respectively.

binary images are displayed in Figs. 10(a-1), 10(b-1), and 10(c-1). Using the binary images in the ImageJ, image analyzer software, the frequency histograms were determined and are shown in Figs. 10(a-2), 10(b-2), and 10(c-2). As can be seen in Figs. 10(a) and 10(b), after strain of 0.2, the microstructure mainly consists of long thin α layers with high AR values in the range of 1.5-3. By increasing the strain value to 0.4, according to Figs. 7(b), 8(b), and 10(b), fragmentation of α_s lamellae starts, leading to decrease in the average length of the layers. The morphological changes caused by fragmentation change the AR frequency histogram (Fig. 10(b-2)) toward a higher frequency of lower AR values, i.e. the range of 1-1.5.

A further increase in the strain value to 0.8 (Figs. 7(c), 8(c), 10(c), and 10(c-1)), significantly increases the fragmentation and spheroidization of α_s lamellae, leading to a more pronounced increase in the frequency of AR values in the range of 1-1.5 (Fig. 10(c-2)). Since, layers with an AR value in the range of 1-1.5 can be considered spherical, the results support previous observations that suggested the progression of spheroidization of α_s lamellae with applied strain.

Using the binary images, i.e. Figs. 10(a-1), 10(b-1), and 10(c-1), the kinetics of α formation can also be studied. The quantitative analysis performed by ImageJ software indicates that the number of alpha layers doubles with the increase in strain from 0.2 to 0.4. In other words, 520 α layers are formed in 20 seconds and the formation rate of the α layers is estimated as 26 layers/s. However, in the strain range of 0.4-0.8, 431 α layers are formed in 40 seconds, and the formation rate

decreases to about 10.8 layers/s. According to these data the rate of α layer formation at low strains (0.2-0.4) is about twice that at high strains (0.4-0.8). This difference in the rate of α layer formation can be attributed to the dominant microstructural mechanism, corresponding to each strain range. As shown in Figs. 7(a, b), 8(a, b), and 10(a, b), in the strain range of 0.2-0.4, deformation mainly contributes to increasing the formation rate of needle-shaped α layers by increasing the number of their nucleation sites. Since the needle-shaped α layers are formed via a quasi-displacive mechanisms, its kinetics is intrinsically fast and become even faster due to the involvement of deformation. However, in the strain range of 0.4-0.8 (Figs. 7(c), 8(c), and 10(c)), deformation activates the fragmentation and spheroidization of α_s layers, which are diffusional processes. Although deformation facilitates diffusion, the inherently slow kinetics of diffusional processes, i.e. fragmentation and spheroidization, appears to be the main reason for the lower rate of α formation at high strain values.

According to Fig. 10(a-2), the number of α layers, whose AR value is in the range of 1-1.5 (i.e., α is almost spherical/spheroidized) is as small as 52 layers. Furthermore, the number of fragmented/spheroidized α layers (AR in the range of 1-1.5) is less than the number of layers with higher AR values, i.e. the second and third categories. This indicates that, not only the fragmentation/spheroidization of previously formed lamellae, but also the formation rate of new α_s layers is very low at $\varepsilon = 0.2$. However, as the strain increases to 0.4 (Fig. 10(b-2)), the number of α layers with an AR value in the range of 1-1.5 has increased to 173, accompanied by a shift of the total AR histogram to lower values. The percentage of α layers with the first three AR categories (1-1.5, 1.5-2, and 2-2.5) at $\varepsilon = 0.2$ and 0.4 is about 42% and 44%, respectively. This indicates a simultaneous fragmentation/spheroidization of previously formed α together with the formation of new short and sharp α_s lamellae. With increasing strain to 0.8 (Fig. 10(c-2)), the number of α layers with low AR values shows a significant increase (reaching 346 layers), which is approximately doubles that at strain 0.4. As the strain increases to 0.8, the contribution of strain to the fragmentation/spheroidization increases, reducing the total AR histogram to the lower AR values, so that the percentage of α layers with an AR value up to 2.5 increases from 44% at $\varepsilon = 0.4$ to 54% at $\varepsilon = 0.8$. Using the AR histograms in Figs. 10(a-2), 10(b-2), and 10(c-2), the rate of fragmentation/spheroidization as a function of applied strain can be estimated. By increasing the strain in the range of 0.2-0.4, the number of α layers with AR values in the range of 1-1.5 increased by 121 layers over a period of 20 seconds. Therefore, the rate of fragmentation/spheroidization is approximately 6 layers/s. A similar analysis shows that with increasing strain in the range of 0.4-0.8, 173 fragmented/spheroidized layers form in 40 seconds, which is equivalent to a rate of 4.3 layers/s. This analysis suggests that the rate of α layer fragmentation/spheroidization is higher in the strain range of 0.2-0.4 than in the strain range of 0.4-0.8. Since, based on the previous results in Figs. 7 and 8, fragmentation/spheroidization mechanisms are not activated sufficiently in the strain range of 0.2-0.4, the increase in the number of α layers with the first three AR values at $\varepsilon = 0.4$ (Fig. 10(b-2)) should be attributed to the formation of new short and sharp α_s layers. Therefore, it is inferred that non-isothermal deformation decreases the average AR value of the α layers by a synergy between the formation of new short and sharp α_s lamellae and the fragmentation/spheroidization of longer α layers. Both mechanisms facilitate the globularization of α and the formation of an equiaxed α + β microstructure.

The effect of non-isothermal deformation on the volume fraction of α_s layers in the deformed samples is shown in Fig. 11. The SEM micrographs of samples deformed to strains of 0.2, 0.4, and 0.8 are shown in Figs. 11(a-c) and the corresponding binary images are displayed in Figs. 11(a-1), 11(b-1), and 11(c-1). The volume fractions of the α phase for the deformed samples up to strains of 0.2, 0.4, and 0.8 were calculated to be 26.4%, 37.6%, and 40.2%, respectively. The gradual increase in the volume fraction of α with applied strain supports the formation of secondary α_s during non-isothermal deformation. The calculated values indicate that the increase in volume fraction in the strain

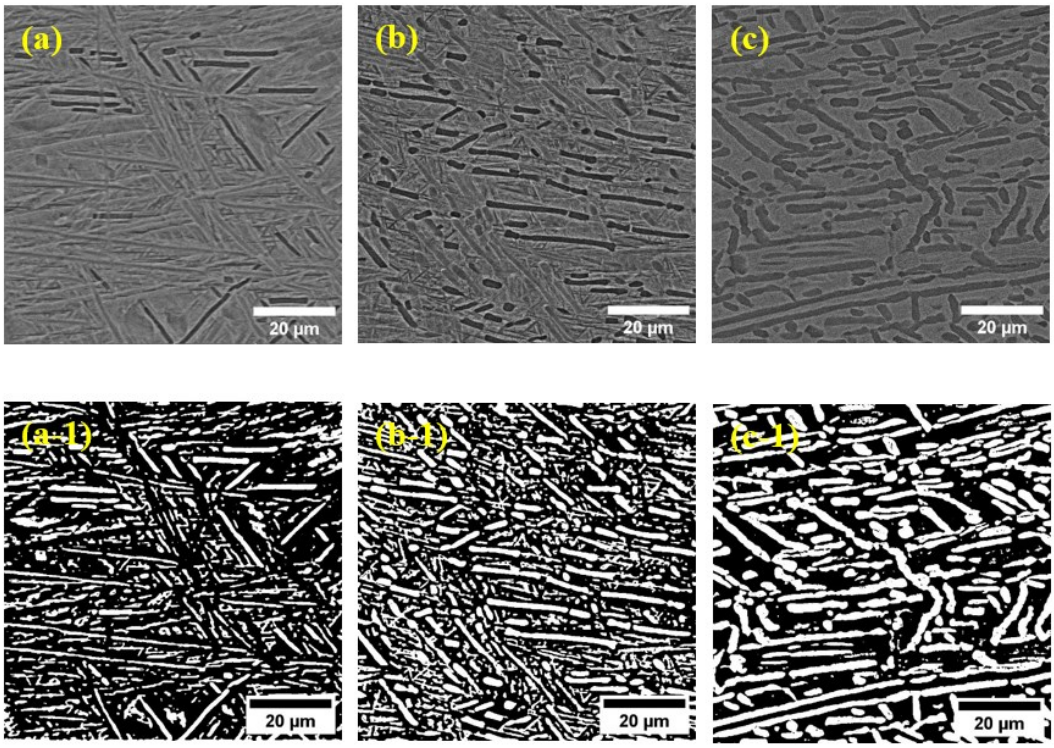

Fig. 11. SEM micrographs from the microstructures of Ti-6Al-4V samples, non-isothermally deformed at a strain rate of 0.01 s^{-1} to strains of (a) 0.2, (b) 0.4, and (c) 0.8. The binary images used to calculate the volume fraction of the alpha layers by ImageJ software for (a), (b), and (c) are presented in (a-1), (b-1), and (c-1), respectively.

range of 0.2-0.4 is greater than that in the strain range of 0.4-0.8. To investigate the reason for this difference, the true stress-strain curve of the material under non-isothermal compression was examined in Fig. 12.

As can be seen in Fig. 12, when the test starts, the stress increases rapidly and reaches a maximum value of about 37 MPa at a strain of ~0.08. The fast increase in dislocation density and the associated work hardening are responsible for the rapid increase in stress to the maximum value [20, 29, 30]. At strains in the range of 0.08-0.3 the stress curve maintains an almost straight line, indicating steady-state flow. A synergy between the temperature drop to about 930 °C (corresponding to ε = 0.3) and deformation leads to the formation of short and sharp α_s lamellae (Figs. 7, 8, and 10). The increase in the total volume fraction of α phase with an HCP structure and the build-up of dislocation in the β_t matrix, increase the rate of work hardening. On the other hand, the fragmentation/spheroidization of the α layers and dynamic softening mechanisms in the matrix act to decrease the rate of work hardening. Accordingly, the steady-state flow in the strain range of 0.08-0.3 is the result of a balance between the factors that increase and those that decrease the work hardening rate [6, 7, 31]. As the strain exceeds 0.3, flow softening replaces the steady-state flow observed at $0.08 \leq \varepsilon \leq 0.3$. The flow softening reduces the flow stress from approximately 37 MPa at ε = 0.3 to about 33 MPa at ε = 0.6 (~11% reduction). Although flow softening in Ti alloys has been attributed to various mechanisms, such as dynamic recovery and recrystallization of β, deformation heating, α-β dynamic transformation and spheroidization of α

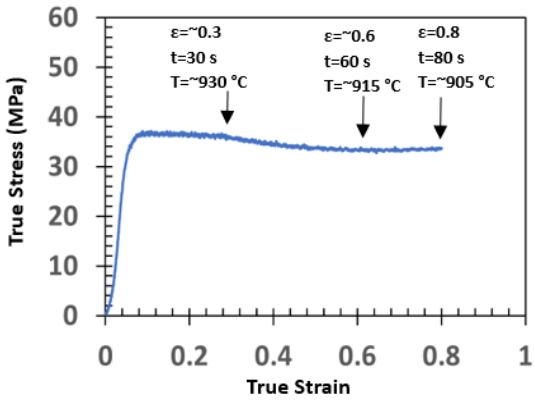

Fig. 12. True stress-true strain curve of the Ti-6Al-4V alloy non-isothermally deformed at strain rate of 0.01 s^{-1}, up to a strain of 0.8.

layers [15, 31, 45, 46], some of them are not applicable to the present alloy. Since a low strain rate was used in this study, the observed flow softening cannot be due to "deformation heating", which usually occurs at high strain rate deformations ($>0.1\ s^{-1}$) [32]. "Dynamic recovery and recrystallization" are the main softening mechanisms in β-Ti alloys and are expected to be very limited in the retained β and β_t [32, 47]. In addition, the contribution of α-β dynamic transformation to the flow softening of Ti-6Al-4V alloy with an initial lamellar microstructure is expected to be very small [22, 33]. Therefore, the formation of secondary α_s and fragmentation/spheroidization of α lamellae, observed in Figs. 7, 8, and 10, appear to be the major source of dynamic softening at strain range of 0.3-0.6. According to Figs. 10(a-1) to 10(c-1), the formation of secondary α_s lamellae as well as the fragmentation/spheroidization of older layers with the applied strain contribute to the increase in the volume fraction and consequently the extent of α/β interfaces. Since, the α/β interfaces act as important sources for the generation of mobile dislocations [34], the increase in their extent through the mentioned mechanisms causes an increase in the mobile dislocations and thereby contributes to the observed flow softening. Furthermore, since the dominant effect of deformation on microstructural changes at low strains is the rotation of the α layers toward the direction perpendicular to the compression axis, the rotation of the layers and their inability to bear the applied load also contribute to steady-state flow in this strain range. At greater strain values, i.e. 0.6-0.8, the flow curve reaches a second steady-state flow, which reflects a new equilibrium between the aforementioned dynamic softening mechanism and the conventional work hardening effect. This equilibrium state represents the weakening of dynamic softening versus work hardening at high strain values. To explain this phenomenon, the following factors may contribute:

- As discussed previously, the rate of increase in the volume fraction of α varies with the applied strain. According to the quantitative analyses in Figs. 10(a-1) to 10(c-1), the increase in the volume fraction of almost spherical α, which is about 42% in the strain range of 0.2-0.4, decreases to about 7% in the strain range of 0.4-0.6. As a consequence, the rate of increase in the volume fraction of α cannot support continued dynamic softening at strains beyond 0.6.
- It was shown that the volume fraction of α_s in the non-isothermally deformed samples is significantly higher than that of the witness sample, cooled at the same cooling rate. The higher volume fraction of α in the non-isothermally deformed samples reduces the supersaturated β matrix and thus decreases the formation rate of new α_s. This, in turn, decreases the rate of increase in the extent of α/β interfaces and therefore weakens the flow softening.
- At high strain values, the misorientation along the sub-boundaries in the α and β phases increases. The thermal grooves, shown in Figs. 8(b) and 8(c), results from the dragging effect exerted by the sub-boundaries with high misorientation angles to the α/β interfaces [4]. Therefore, this process competes with the formation of new α_s lamellae in consuming the stored deformation energy and therefore reduces the rate of increase in the volume fraction of α [15, 35]. With increasing strain to 0.8, the thickness of α_s increases due to growth. As a result, the fragmentation of layers via buckling or shear is no longer dominant and thus rapid fragmentation loses its effectiveness. Instead, the diffusion of β through the thermal grooves leads to the subdivision of the α layers. In other words, boundary splitting through an inherently slow diffusional mechanism is responsible for the fragmentation in this condition [36, 38]. Under weak spheroidization and slow formation of new α_s layers, the flow softening cannot overcome the work hardening. Consequently, the two processes reach an equilibrium state, which appears as a straight line on the flow curve.

3.3. The effect of strain in inducing secondary alpha in non-isothermal deformation

Fig. 13 shows the SEM microstructures of the witness sample after two-phase heat treatment at 950 °C for 5 minutes and quenching to ambient temperature (point B

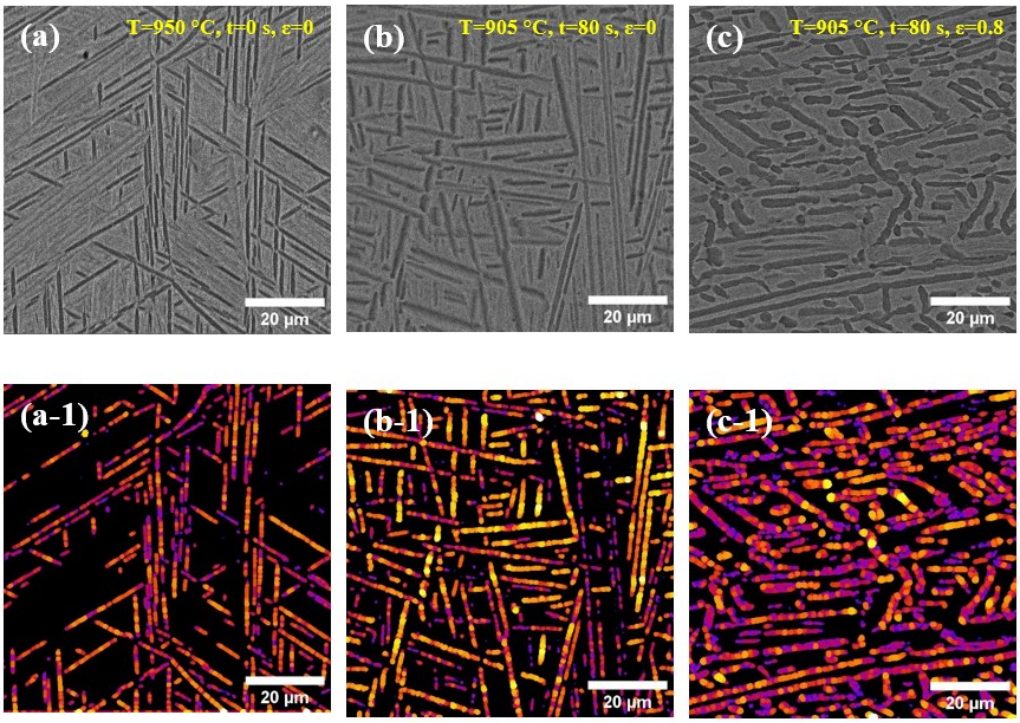

Fig. 13. SEM microstructures of (a) the witness sample before non-isothermal deformation, held at 950 °C for 5 minutes (point B in Fig. 2), (b) the witness sample cooled for 80 seconds without deformation (corresponding to $\varepsilon = 0.8$) with a cooling rate of 0.6 °C/s, and (c) the sample non-isothermally deformed up to $\varepsilon = 0.8$ with a strain rate of 0.01 s^{-1}. Figs. (a-1), (b-1), and (c-1) represent the thickness distribution of the α layers corresponding to Figs. (a), (b), and (c), respectively.

in Fig. 2), the witness sample after cooling for 80 seconds (corresponding to $\varepsilon = 0.8$) without deformation and the sample non-isothermally deformed to $\varepsilon = 0.8$ at a strain rate of 0.01 s^{-1}. The volume fraction of α in the witness sample before non-isothermal deformation (Fig. 13(a)) is estimated to be about 20.3%. In the witness sample continuously cooled for 80 seconds at a cooling rate of 0.6 °C/s, the volume fraction of α increases to 29.7% (Fig. 13(b)). This increase in α percentage is solely due to the decrease in temperature from 950 °C to about 905 °C. In other words, a temperature drop of about 50 °C leads to a 9.4% increase in the volume fraction of the α phase. However, Fig. 13(c) indicates that the same temperature drop together with a strain of 0.8 increases the α volume fraction to 40.2%, which is about twice that observed in Fig. 13(a) and 1.35 times that in Fig. 13(b). The difference in the α volume fraction between the cooled witness sample and the non-isothermally deformed sample is about 10.5%, which is solely attributable to deformation. Therefore, it can be stated that cooling and deformation have comparable effects on promoting α phase formation, and their combined effect nearly doubles the volume fraction of α relative to the two-phase annealed condition. The acceleration of α precipitation in the deformed samples suggests that deformation features, especially dislocations, facilitate diffusion and provide additional nucleation sites for the formation of α layers [6, 39, 40-42]. Furthermore, the deformation concomitant with the precipitation of α_s disrupts the Burgers orientation relationship between α and β, promoting a morphological transformation from a lamellar to an equiaxed structure [6].

The thickness distributions of the α layers in Figs. 13(a-1) to 13(c-1) indicate that the average thickness of the α layers in Figs. 13(a), 13(b), and 13(c) is 1.4, 2.3, and 3.8 µm, respectively.

The increase in the holding time at high temperature is the reason for the higher average thickness of the α layers in the cooled witness sample and the non-isothermally deformed sample (Figs. 13(b-1) and 13(c-1)) relative to the two-phase annealed sample (Fig. 13(a-1)).

A comparison between Figs. 13(b-1) and 13(c-1) suggests that deformation increases the volume fraction of α_s as well as the average thickness of the α_s layers. The increase in the number of α_s layers in the deformed sample decreases the average inter-layer distance. The applied deformation also activates thermal grooving, fragmentation of the layers and their spheroidization through the termination migration and Ostwald ripening mechanisms (Fig. 13(c-1)). With increasing strain, the number of dislocations in the α phase increases, leading to enhanced pipe diffusion through the dislocation cores. Therefore, the increased elemental diffusion through the dislocations is the major reason for the observed increase in the average thickness of the α_s layers in the deformed sample [6, 8, 43].

4. Conclusion

In the present study, the non-isothermal deformation behavior of Ti-6Al-4V alloy and the effect of strain on its microstructural evolutions were investigated. For this purpose, samples were compressed at a constant strain rate of 0.01 s^{-1} under non-isothermal conditions with a cooling rate of about 0.6 °C/s, starting from 950 °C to strain levels of 0.2, 0.4, and 0.8. The main findings of this study are summarized below:

1) During non-isothermal deformation, the main microstructural components are: transformed beta phases (β_t), primary alpha (α_p), secondary alpha (α_s), and retained beta.
2) During non-isothermal deformation, the volume fraction of the secondary alpha lamellae increases significantly with increasing applied strain. Regardless of the temperature drop, deformation promotes the formation of numerous fine, needle-shaped secondary alpha lamellae. The microstructural observations showed that the volume fraction of alpha lamellae increased by about 10.5%, in the sample deformed to a strain of 0.8.
3) The secondary alpha phases induced by temperature reduction are often lamellar. In contrast, the application of strain promotes the formation of a greater number of acicular secondary alpha phases.
4) As the strain increases, the aspect ratio of the secondary alpha layers decreases. Consequently, at a strain of 0.8, 54% of the alpha lamellae exhibit an aspect ratio of less than 2.5.
5) At low applied strains (up to 0.4), the dominant effect of strain is to increase the volume fraction of secondary alpha, and the prevailing mechanism of alpha-lamella spheroidization is fragmentation through buckling. However, at higher strains (from 0.4-0.8), the dominant deformation mechanism shifts, and spheroidization of the alpha lamellae mainly occurs through the formation of thermal grooves and boundary splitting.
6) At lower applied strains (0.2 to 0.4), the rates of secondary alpha formation and spheroidization are higher than those observed at higher applied strains (0.4-0.8).

Authors' contributions

M. Jafari: Methodology, Conceptualization, Data curation, Formal analysis, Visualization, Investigation, Writing

G. Ebrahimi: Supervision, Validation, Writing - original draft

S. M. Fatemi: Supervision, Validation, Writing - original draft

A. Momeni: Co-supervisor, Review & editing

M. Mazinani: Co-supervisor

Conflict of interest

The authors declare no conflict of interest.

Funding

This research was funded by Ferdowsi University of Mashhad.

5. References

[1] Bambach, M. D., Seiferta, D., & Sizov, I. (2020). Intensive forming of grade 5 titanium bars with increased performance for aerospace applications. *Procedia Manufacturing, 47*, 288-294. https://doi.org/10.1016/j.promfg.2020.04.229

[2] Liu, C. C., Li, Y. H. Z., Gu, J., & Song, M. (2024). Phase transformation in titanium alloys: A review.

Transactions of Nonferrous Metals Society of China, 34(10), 3039-3117. https://doi.org/10.1016/S1003-6326(24)66597-0

[3] Gao, P., Fu, M., Zhan, M., Lei, Z., & Li, Y. (2020). Deformation behavior and microstructure evolution of titanium alloys with lamellar microstructure in hot working process: A review. *Journal of Materials Science & Technology, 39*, 56-73. https://doi.org/10.1016/j.jmst.2019.07.052

[4] Zhang, J., Li, H., & Zhan, M. (2020). Review on globularization of titanium alloy with lamellar colony. *Manufacturing Review*, *7*, 18. https://doi.org/10.1051/mfreview/2020015

[5] Kim, J. Y., Park, K. T., Shim, I. O., & Hong, S. H. (2008). Globularization behavior of ELI grade Ti-6Al-4V alloy during non-isothermal multi-step forging. *Materials Transactions, 49*(1), 215-223. https://doi.org/10.2320/matertrans.MER2007224

[6] Fan, X. G., Meng, M., Gao, P. F., & Zhan, M. (2018). Coupled effects of deformation and cooling on the evolution of primary and secondary alpha of two-phase Ti-alloys. *Materials Science & Engineering: A*, *710*, 271-279. https://doi.org/10.1016/j.msea.2017.10.106

[7] Li, J., Li, X., Cao, F., Li, Z., Chen, P., & Chen, L. (2024). Effect of deformation and cooling on non-equilibrium microstructure evolution and phase transition mechanism of Ti-6Al-2.5V-1.5Cr-0.5Fe-0.3Si. *Journal of Materials Research and Technology*, *33*, 6656-6666. https://doi.org/10.1016/j.jmrt.2024.11.044

[8] Li, J., Wang, A., Li, X., Chen, P., Wang, B., & Li, Z. (2025). Evolution of secondary α phase in TC6 alloy under different deformation and cooling conditions in non-isothermal deformation. *Journal of Alloys and Compounds, 1040*, 183480. https://doi.org/10.1016/j.jallcom.2025.183480

[9] Chen, J., Li, J., Tang, B., Chen, Y., & Kou, H. (2019). Microstructure and texture evolution of a near β titanium alloy Ti-7333 during continuous cooling hot deformation. *Progress in Natural Science: Materials International, 29*(1), 50-56. https://doi.org/10.1016/j.pnsc.2019.01.003

[10] Meng, M., Fan, X. G., Yang, H., Guo, L. G., Zhan, M., & Gao, P. F. (2017). Precipitation of secondary alpha in competition with epitaxial growth of primary alpha in two-phase titanium alloys. *Journal of Alloys and Compounds, 714*, 294-302. https://doi.org/10.1016/j.jallcom.2017.04.209

[11] Lu, H., Wang, S., Mi, C., Zhang, H., Guo, Y., Zhang, S., & Zhang, X. (2024). The space of secondary α phase significantly affects the mechanical properties of metastable β-type Ti-4V-2Mo-2Fe alloy. *Materials Letters, 373*, 137148. https://doi.org/10.1016/j.matlet.2024.137148

[12] Ji, X., Yu, H., Guo, B., Jiang, F., Fu, D., Teng, J., Zhang, H., & Jonas, J. J. (2020). Post-dynamic α to β phase transformation and reverse transformation of Ti-5Al-3V alloy after hot deformation in two phase region. *Materials and Design, 188*, 108466. https://doi.org/10.1016/j.matdes.2019.108466

[13] Xu, S., Zhang, H., Xiao, N., Qiu, R., Cui, Z., & Fu, M. (2023). Mechanisms of macrozone elimination and grain refinement of near α Ti alloy via the spheroidization of the Widmannstätten structure. *Acta Materialia, 260*, 119339. https://doi.org/10.1016/j.actamat.2023.119339

[14] Liang, Z., Miao, J., Huang, X., Zhang, F., Williams, J. C., & Luo, A. A. (2022). Kinetically induced fine secondary α-Ti phase formation in a novel as-cast titanium alloy. *Metallurgical and Materials Transactions A, 53*(10), 3536. https://doi.org/10.1007/s11661-022-06775-2

[15] Banerjee, D., Pilchak, A., & Williams, J. C. (2012). Processing, structure, texture and micro-texture in titanium alloys. *Materials Science Forum, 710*, 66-84. https://doi.org/10.4028/www.scientific.net/MSF.710.66

[16] Lin, Y. C., Xiao, Y. W., Jiang, Y. Q., Pang, G. D., Li, H. B., Zhang, X. Y., & Zhou, K. C. (2020). Spheroidization and dynamic recrystallization mechanisms of Ti-55511 alloy with bimodal microstructures during hot compression in α + β region. *Materials Science & Engineering: A, 782,* 139282. https://doi.org/10.1016/j.msea.2020.139282

[17] Meng, M., Fan, X. G., Gao, P. F., Guo, L. G., Zhan, M., & Wei, K. (2017). Microstructure evolution in near isothermal forming of titanium alloy component. *Procedia Engineering, 207*, 2173-2178. https://doi.org/10.1016/j.proeng.2017.10.977

[18] Kedia1, B., Balasundar, I., & Raghu, T. (2018). Globularisation of α lamellae in titanium alloy: Effect of strain, strain path and starting microstructure. *Transactions of the Indian Institute of Metals, 71*(7), 1791-1801. https://doi.org/10.1007/s12666-018-1323-y

[19] Chong, Y., Bhattacharjee, T., Gholizadeh, R., Yi, J., & Tsuji, N. (2019). Investigation on the hot deformation behaviors and globularization mechanisms of lamellar Ti-6Al-4V alloy within a wide range of deformation temperatures. *Materialia, 8*, 100480. https://doi.org/10.1016/j.mtla.2019.100480

[20] Xu, X., Zhang, B., Xue, J., Li, F., Su, S., & Chang, H. (2024). Microstructural characteristics and

recrystallization mechanism of Ti-6.5Al-2Zr-1Mo-1V alloy during two-stage hot deformation. *Journal of Materials Research and Technology, 30*, 769-781. https://doi.org/10.1016/j.jmrt.2024.03.120

[21] Zhang, J., Xu, X., Xue, J., Liu, S., Deng, Q., Li, F., Ding, J., Wang, H., & Chang, H. (2022). Hot deformation characteristics and mechanism understanding of Ti-6Al-2Sn-4Zre-6Mo titanium alloy. *Journal of Materials Research and Technology, 20*, 2591-2610. https://doi.org/10.1016/j.jmrt.2022.08.044

[22] Zherebtsov, S., Murzinova, M., Salishchev, G., & Semiatin, S. L. (2011). Spheroidization of the lamellar microstructure in Ti-6Al-4V alloy during warm deformation and annealing. *Acta Materialia, 59*(10), 4138-4150. https://doi.org/10.1016/j.actamat.2011.03.037

[23] Germain, L., Gey, N., Humbert, M., Vo, P., Jahazi, M., & Bocher, P. (2008). Texture heterogeneities induced by subtransus processing of near α titanium alloys. *Acta Materialia, 56*(16), 4298-4308. https://doi.org/10.1016/j.actamat.2008.04.065

[24] Tamizifar, M., Omidvar, H., Salehi, S. M. T., Salehpour, Z., & Khoshkalam, O. (2002). Effect of processing parameters on shear bands in non-isothermal hot forging of Ti-6Al-4V. *Materials Science and Technology,18*(1), 21-29. https://doi.org/10.1179/026708301125000168

[25] Oh, J. M., Hong, J. K., Yeom, J. T., Lee, S. W., Kim, E. Y., Kang, N., & Park, C. H. (2020). Accelerated formation of an ultrafine-grained structure in a two-phase Ti alloy during compression with decreasing temperatures. *Philosophical Magazine, 100*(12), 1569-1584. https://doi.org/10.1080/14786435.2020.1728414

[26] Li, R., Ding, Y., Ji, R., Chen, L., & Mao, J. (2025). The accelerated globularization kinetics of titanium alloys with lamellar microstructure: A brief review. *Journal of Materials Science, 60*(1), 98-117. https://doi.org/10.1007/s10853-024-10536-4

[27] Gao, P. F., Yang, H., Fan, X. G., & Yan, S. L. (2012). Microstructure evolution in the local loading forming of TA15 titanium alloy under non-isothermal condition. *Journal of Materials Processing Technology, 212*(11), 2520-2528. https://doi.org/10.1016/j.jmatprotec.2012.04.019

[28] Zhu, S., Yang, H., Guo, L. G., & Fan, X. G. (2012). Effect of cooling rate on microstructure evolution during α/β heat treatment of TA15 titanium alloy. *Materials Characterization, 70*, 101-110. https://doi.org/10.1016/j.matchar.2012.05.009

[29] Callegari, B., Oliveira, J. P., Coelho, R. S., Brito, P. P., Schellf, N., Solder, F. A., Mücklich, F., Sadikg, M. I., Garcíag, J. L., & Pinto, H. C. (2020). New insights into the microstructural evolution of Ti-5Al-5Mo-5V-3Cr alloy during hot working. *Materials Characterization, 162*, 110180. https://doi.org/10.1016/j.matchar.2020.110180

[30] Banerjee, D., & Williams, J. C. (2013). Perspectives on titanium science and technology. *Acta Materialia, 61*(3), 844-879. https://doi.org/10.1016/j.actamat.2012.10.043

[31] Kim, Y., Young, H. J., Park, J., Kim, K., Kwon, H., Ju, G., & Kim, N. (2023). Optimizing process parameters for hot forging of Ti-6242 alloy: A machine learning and FEM simulation approach. *Journal of Materials Research and Technology*, *27*, 8228-8243. https://doi.org/10.1016/j.jmrt.2023.11.193

[32] Perumal, B., Rist, M. A., Gungor, S., Brooks, J. W., & Fitzpatrick, M. E. (2016). The effect of hot deformation parameters on microstructure evolution of the α-phase in Ti-6Al-4V. *Metallurgical and Materials Transactions A, 47*(8), 4128-4136. https://doi.org/10.1007/s11661-016-3552-1

[33] Guo, B., Semiatin, S. L., & Jonas, J. J. (2019). Dynamic transformation during the high temperature deformation of two-phase titanium alloys. *Materials Science & Engineering A, 761*, 138047. https://doi.org/10.1016/j.msea.2019.13804

[34] Fan, X. G., Yang, H., & Gao, P. (2014). The mechanism of flow softening in subtransus hot working of two-phase titanium alloy with equiaxed structure. *Chinese Science Bulletin, 59*(23), 2859-2867. https://doi.org/10.1007/s11434-014-0332-4

[35] Luo, J., Ye, P., Han, W. C., & Li, M. Q. (2018). Collaborative behavior in α lamellae and β phase evolution and its effect on the globularization of TC17 alloy. *Materials and Design, 146*, 152-162. https://doi.org/10.1016/j.matdes.2018.03.020

[36] Wang, L., Fan, X. G., Zhan, M., Jiang, X. Q., Liang, Y. F., Zheng, H. J., & Liang, W. J. (2021). Revisiting the lamellar globularization behavior of a two-phase titanium alloy from the perspective of deformation modes. *Journal of Materials Processing Technology, 289*, 116963. https://doi.org/10.1016/j.jmatprotec.2020.116963

[37] Li, X., Ouyang, D., & Zhang, K. (2024). Hot deformation characteristic of TC21 titanium alloy with lamellar microstructure. *Materials Today Communications, 39,* 108709. https://doi.org/10.1016/j.mtcomm.2024.108709

[38] Sua, J., Jia, X., Xiea, H., Tanga, J., Jianga, F., Fua, D., Tenga, J., & Zhang, H. (2022). Constitutive and microstructural characteristics of Ti-5Al-2.5Sn alloy during isothermal and non-isothermal multi-stage hot deformation across different phase regions. *Journal of Alloys and Compounds, 908*, 164647. https://doi.org/10.1016/j.jallcom.2022.164647

[39] Zhang, Y., Jiang, Y., Si, K., Xin, S., Zhang, S., Hou, F., Zhang, K., Hai, J., Xiao, L., Yang, Y., Wang, H., Huang, A., & Zhang, L. C. (2024). Microstructure refinement induced by elastic compressive stress in Ti-6Al-4V alloy. *Journal of Alloys and Compounds, 981*, 173700. https://doi.org/10.1016/j.jallcom.2024.173700

[40] Wang, K., & Li, M. Q. (2014). Effects of heat treatment and hot deformation on the secondary α phase evolution of TC8 titanium alloy. *Materials Science and Engineering: A, 613*, 209-216. https://doi.org/10.1016/j.msea.2014.06.056

[41] Yu, W. X., Li, M. Q., & Luo, J. (2010). Effect of deformation parameters on the precipitation mechanism of secondary α phase under high temperature isothermal compression of Ti-6Al-4V alloy. *Materials Science and Engineering: A, 527*(16-17), 4210-4217. https://doi.org/10.1016/j.msea.2010.03.024

[42] Xu, J., Zeng, W., Zhu, Z., Li, M., Du, J., He, S., & Wang, X. (2023). Precipitation and evolution behaviors of grain boundary α and α side plates for ultra-high strength titanium alloy during continuous cooling. *Materials & Design, 225*, 111562. https://doi.org/10.1016/j.matdes.2022.111562

[43] Guo, Y., Dong, R., Li, C., Yang, L., Hou, H., & Zhao, Y. (2025). Microstructural evolution and mechanical properties of an (α + β) titanium alloy subjected to cyclic multi-directional forging. *Materials Characterization, 230*, 115772. https://doi.org/10.1016/j.matchar.2025.115772

[44] Abbasi, S. M., & Momeni, A. (2011). Effect of hot working and post-deformation heat treatment on microstructure and tensile properties of Ti-6Al-4V alloy. *Transactions of Nonferrous Metals Society of China, 21*, 1728-1734. https://doi.org/10.1016/S1003-6326(11)60922-9

[45] Momeni, A., Abbasi, S. M., & Morakabati, M. (2016). Flow softening behavior of Ti-13V-11Cr-3Al beta Ti alloy in double-hit hot compression tests. *Journal of Materials Research*, *31*, 3900-3906. https://doi.org/10.1557/jmr.2016.430

[46] Abbasi, S. M., Momeni, A., Lin, Y. C., & Jafarian, H. R. (2016). Dynamic softening mechanism in Ti-13V-11Cr-3Al beta Ti alloy during hot compressive deformation. *Materials Science and Engineering: A*, *665*, 154-160. https://doi.org/10.1016/j.msea.2016.04.040

[47] Kulakov, M., Rahimi, S., & Semiatin, S. L. (2021). Effect of deformation heating on microstructure evolution during hot forging of Ti-6Al-4V. *Metallurgical and Materials Transactions A*, *53*(2), *407-419*. https://doi.org/10.1007/s11661-021-06493-1